Research Article

Daniel Van Opdenbosch*, Martin Kretschmer, Oliver Lieleg, and Cordt Zollfrank

Free volumes in mixed-tacticity poly(3-hydroxybutyrate) determined by viscosimetry and their correlations with structural features and mechanical properties

https://doi.org/10.1515/arh-2022-0125
received September 17, 2021; accepted June 17, 2022

Abstract: The viscosities of poly(3-hydroxybutyrate) (PHB) with mixed tacticities were determined as functions of temperature and shearing rate via plate–plate viscosimetry, and fitted by a combined Herschel–Bulkley–Cross–Doolittle model while applying Carvalho et al.'s single-point correction. They were compared to values of slit viscosimetry, obtained during processing at a temperature of 428 K. In both cases, measured values and fitted model parameters as a function of tacticity exhibited a discontinuous behaviour at a fraction of meso diads of 0.7. To further investigate, we calculated values of vibrational and excess free volume. We found that these correlate with structural and external properties, some of which were reported in earlier works, namely the paracrystalline contents and specific volumes of the materials at room temperature, as well as their energies of fracture during tensile testing. These, in turn, correlate with the statistical averages of relative lengths of chain segments of similar a- or iso-tacticity. Hence, we found that expressing changing tacticities simply by a continuous progression of the fraction of meso diads is insufficient to trace associated discontinuities of the flow behaviour in mixed-tacticity PHB. We conclude that free volume is generated by polymer chain conformational disorder, which should be treated on the oligomeric chain segment level.

Keywords: poly(3-hydroxybutyrate), tacticity, viscosity, free volume, thermal expansion

1 Introduction

1.1 Mixed-tacticity poly(3-hydroxybutyrate) (PHB)

In order to trace the development of the resulting structural features and mechanical properties, we recently synthesized mixed-tacticity variants of PHB [1]. Since it is readily and securely determinable by NMR, we used the fraction of meso diads, f_{meso}, as their characteristic figure. We further determined that changes in mechanical properties [2] with f_{meso} correlate with the thermal expansion coefficients and therefore with the amounts of free volume generated by vibrational motions [3].

During the injection moulding of samples for mechanical testing with a twin-screw extruder, as reported earlier [2], we also noted that the screw momenta progressed nonlinearly from batch to batch with f_{meso}. In general, rheological properties of polymers arise from – and therefore reveal – fundamental structural features. We hypothesized that the development of free volume with mixed tacticity would be reflected in key rheological and mechanical figures. Since both are a result of mixed main-chain tacticities, we further hypothesized that the amount of free volume and the proportion of material exhibiting paracrystalline disorder [4] might be correlated.

Hence, in this work, we consider the rheological properties of mixed-tacticity PHB melts, both in a laboratory and a processing context. Specifically, we performed plate–plate rheology measurements on samples from a

* **Corresponding author: Daniel Van Opdenbosch,** Chair for Biogenic Polymers, Campus Straubing for Biotechnology and Sustainability, Technical University of Munich, Schulgasse 16, D-94315 Straubing, Germany, e-mail: daniel.van-opdenbosch@tum.de
Martin Kretschmer, Oliver Lieleg: Chair for Biomechanics, Department of Mechanical Engineering, Technical University of Munich, Boltzmannstrasse 11, D-85748 Garching, Germany
Cordt Zollfrank: Chair for Biogenic Polymers, Campus Straubing for Biotechnology and Sustainability, Technical University of Munich, Schulgasse 16, D-94315 Straubing, Germany

range of $0.55 \leq f_{meso} \leq 1$ and evaluated the data recorded by the extruder.

1.2 Polymer viscosity and free volumes

The Arrhenius-type Glasstone et al. [5], Williams et al. [6], and Doolittle [7,8] equations are commonly used to model the dependence of polymer viscosities on the temperature T. The latter gives immediate physical meaning to the flow activation energy via the concept of free volumes V_{free}, equation (1), as also reviewed by Wang and Porter [9]. For a comprehensive review of the different implementations of the concept, we refer to Lipson and White, whose nomenclature we use in the following equations [10]:

$$\eta_0(T) = A \exp(BV_{hc} / V_{free}(T)), \quad (1)$$

$$V_{hc} = V(T) - V_{free}(T), \quad (2)$$

$$V_{free}(T) = V_{free:vib}(T) + V_{free:exs}(T), \quad (3)$$

$$V_{free:vib}(T) = \alpha_g T V_{hc}, \quad (4)$$

$$V_{free:exs}(T) = \alpha_l (T - T_g) V_{vib}(T), \quad (5)$$

$$V_{vib}(T) = V_{hc} + V_{free:vib}(T), \quad (6)$$

where V_{hc} is the incompressible "hard-core" volume, $V_{free}(T)$ and $V_{free}(T)/V_{hc}$ are the total and relative free volumes as functions of temperature T, $V(T)$ is the total volume (with solid-state portion V_{vib}), $V_{free:vib}$ the free volume generated by thermal vibrations, and $V_{free:exs}$ the "excess" free volume generated by liquid motion. α_g and α_l are the volume expansion coefficients of the material in its glassy and liquid states, i.e. below and above the glass transition temperature T_g. A and B are empirical parameters that are constant for a single substance [7,9].

Using equations (2)–(6) to account for contributions of vibrational- and liquid motions as initially proposed by Fox and Flory [11,12] leads to the form for $V_{free}(T)$ applied in this work and valid above T_g, equation (7). Expressed in words, it gives the total free volume as the sum of the vibrational- ("glassy," for continuity) and the liquid motion expansion coefficients α_g and α_l, both acting on the hard core volume, and α_l also acting on the free vibrational volume $V_{free:vib} \propto \alpha_g T$. This correlation retains the nonlinear increase predicted by the locally corrected lattice model by White et al. [13] and Lipson and White [14]. As a note, in measurements performed under pressure P, the exponential term may require the appendage of a correction parameter $\exp(\ldots + \beta P)$ [15].

Inserting equation (7) into equation (1) yields equation (8). In the literature, equation (8) is often given in simplified form $\eta = A \exp(B/(\alpha_l(T - T_0)))$ [9]. Here, T_0 is a "virtual" glass transition point [16] and often fixed [9]. This approach reduces the number of fitting parameters, thereby increasing the robustness of the remaining parameters. Furthermore, deviations of T_0 from T_g can be used to account for amounts of $V_{free:exs}$ frozen in during rapid cooling below the glass transition temperature. However, prior knowledge of α_g can be used to circumvent a lack of robustness. To account for the dependence on the shear rate $\dot{\gamma}$ and for yield shear stress, one may insert equation (8) into a combined Herschel and Bulkley [17] and Cross [18] model, resulting in equation (9).

$$V_{free}(T) = (\alpha_g T + \alpha_g T \alpha_l (T - T_g) + \alpha_l (T - T_g)) V_{hc}, \quad (7)$$

$$\eta_0(T) = A \exp(B/(\alpha_g T + \alpha_g T \alpha_l (T - T_g) + \alpha_l (T - T_g))), \quad (8)$$

$$\eta(T, \dot{\gamma}) = \tau_0 \exp(T_\tau / T)/\dot{\gamma} + \eta_0(T)/(1 + (\eta_0(T)\dot{\gamma}/\tau^*)^{1-n}), \quad (9)$$

where τ_0 and τ^* are the yield shear stress, and the critical shear stress during the transition between Newtonian and shear thinning region ("Hookean shear modulus" of viscoelastic fluids in the original) [19]. The temperature dependence of the yield stress is accounted for by T_τ. n is the flow behaviour index, indicating Newtonian behaviour as $n = 1$, shear thinning as $n < 1$, or shear thickening as $n > 1$.

We evaluated temperature- and shear rate-resolved rheometric data on the basis of equation (9). Two aims were followed: First, to generally elucidate the changes of flow behaviour with changing PHB main-chain tacticity, as expressed by f_{meso}. Second, to trace characteristic parameters describing the observed flow behaviour to tacticity-dependent structural features determined recently [3,4].

2 Experimental section

2.1 Polymer synthesis

The manner of polymer synthesis has been reported earlier [1]. In brief, S- and R-β-butyrolactone monomers were polymerized with defined fractions of R, $0.5 < f_R \leq 1$. We utilized ethylzinc β-diketiminate as a catalyst and 4-methoxybenzyl alcohol as a co-catalyst in dry toluene under stirring for 24 h at 80°C, using standard Schlenk techniques. The reactions were quenched with small amounts of methanol, ground with a mortar, and washed with methanol. All materials were used as synthesized and after ageing for at least 7 days. Purely

isotactic PHB was also obtained from microbial cultures (Biomer, Krailing, Germany).

We determined the fraction of meso diads f_{meso} for each prepared material from nuclear magnetic resonance spectroscopy [1]. Since they are fixed properties of the PHB chains themselves, they were subsequently used as their descriptor. Due to the spacing between the assessed f_{meso}, characteristic values or ranges are naturally approximates with an uncertainty given by the distance between adjacent data points. Hence, any statement "$f_{meso}(<,=,>)x$" means "$f_{meso}(\lesssim, \approx, \gtrsim)x$," with the aforementioned uncertainty.

2.2 Plate–plate viscosimetry

Rheological measurements were performed using a commercial rheometer (MCR 302; Anton Paar, Graz, Austria) with a 8 mm plate–plate geometry (PP08 measuring head, Anton Paar) and therefore a radius $R = 4$ mm, and a plate separation $h = 0.3$ mm. The torque M was measured in dependence of both the temperature and shear rate for each sample. Solid PHB samples were placed onto the rheometer plate (P-PTD 200/AIR, Anton Paar) and molten by a temperature treatment; here, a temperature level of at least 25 K above the melting point of the respective sample was chosen. Per composition f_{meso}, four samples from typically four, but at least two different synthesis batches each were measured.

After lowering the measuring head, the samples were trimmed by use of a metal spatula. Then, the temperature was reduced to a level slightly above the "gel" point of the respective sample, which in each case corresponded roughly to its melting point T_m, as determined earlier [2]. The maximum temperature used was 460 K. To reach these temperatures, a heating hood (H-PTD200, Anton Paar) was used. Measurements were started after a tempering time of 20 min.

The temperature was increased in increments of 10 K. At each temperature, the viscosity was determined in rotational mode in a rotational frequency range $1\ s^{-1} > f > 0.01\ s^{-1}$; ten measuring points were acquired per decade. Before each shear ramp, the sample was exposed to a constant shearing of $f = 1\ s^{-1}$ for 5 min to temper the sample and to exclude boundary effects. Thus, we obtained values of M, spanning the parameter space of $f_{meso} \times T \times f$.

We expected non-Newtonian behaviour and therefore considered the actual shear stress progression with plate radius. Since the flow behaviour indices were not known beforehand, we implemented Carvalho et al.'s single-point correction into the fitting routine (described in the following) [20]. We calculated and report the viscosities at the particular radius $r_s = r_s^* R$, equation (10).

$$\eta\left(\dot{\gamma}_{r_s}\right) = \tau_{r_s} / \dot{\gamma}_{r_s}, \tag{10}$$

$$\tau_{r_s} = r_s^* \tau_{0,R}, \quad \dot{\gamma}_{r_s} = r_s^* \dot{\gamma}_R, \tag{11}$$

$$\tau_{0,R} = 2M / (\pi R^3), \tag{12}$$

$$\dot{\gamma}_R = \Omega R / h, \tag{13}$$

$$r_s^* = (4/(3+n))^{1/(n-1)}.$$

Here, $\Omega = 2\pi f$ is the angular velocity and M is the measured torque. Equations (12) and (13) provide the apparent shear stress and the shear rate, and therefore the apparent Newtonian viscosity at the plate rim, which are corrected to the values at the particular radius by equation (11). While r_s^* cancels out in equation (10), the correction is required to map the apparent values $\eta_0(\dot{\gamma}_R) = \tau_{0,R} / \dot{\gamma}_R$, i.e. at rim condition, to the shear rates $\dot{\gamma}_{r_s}$ at which they actually occur. Implementing the single-point correction in the fitting routine adds robustness to the iterative determination of n: Any progression of $\eta(\dot{\gamma}_{r_s})$ is altered at worst by 4% from the Newtonian values for any $0 \le n \le 1.2$ [20], but in return represents a closer approximation of the actual values.

To the data $\eta(T, \dot{\gamma}_{r_s})$, the model given by equation (9) was fitted per f_{meso} by a least-squares trust region reflective algorithm (Lmfit, Python) [21], while performing the single-point correction for each iteration, and applying only mathematically or physically required boundaries and uniform starting conditions, including previously determined values of α_g [1–3]. During fitting trials, we found that the data obtained in this work required treating the flow behaviour index as a function of temperature, starting from a high-temperature limit n_0, as follows:

$$n = n_0 / \exp(C / (T - T_n)), \tag{14}$$

where C is an empirical constant similar to B in its effect. T_n accounts for the temperature effect on n, similar to T_τ. We found that both can be treated as one parameter without loss of fitting quality. Hence, we applied the respective T_m as the values for T_τ and T_n in equations (9) and (14) as follows:

$$T_\tau \equiv T_n \equiv T_m. \tag{15}$$

Alternative explanations, such as a temperature dependence of τ^* did not result in the same fitting quality, nor did applying power law, Carreau–Yasuda or Bingham equations [22].

Equation (8) assumes a homogeneous amorphous material with α_g and α_l valid for the entire bulk.

For semicrystalline materials, the progression of the true bulk volume above T_g progresses at a flatter trajectory than given by α_l. Above the melting temperature T_m, it increases sharply to join the curve projected for an amorphous phase. Hence, the development of $V_{free:exs}$ is effectively delayed to higher temperatures. Within the context of our work, this detail is not of importance, since we measured all polymer compositions above their respective T_m [2].

All measurements were performed with great care. Nonetheless, we wished to make the reported values robust against potential measurement errors, such as gas entrapments, incomplete homogenization, underfilling, and overfilling. Hence, we uniformly used medians and median absolute deviations to group and provide uncertainties to measurement values or calculation results pertaining to the same parameters.

2.3 Slit viscosimetry

In an earlier work [2], we used a twin-screw extruder (HAAKE Minilab II; Thermo Fisher Scientific, Karlsruhe, Germany) to produce samples for mechanical testing. Here, synthesized mixed-tacticity PHB with $f_{meso} < 1$ and the microbial reference were used. Prior to extrusion, carried out at 428 K and 50 twin-screw revolutions per minute, the melts were circulated through the bypass channel for 10 min to homogenize. During this process, the following data were collected over time: The momenta M required to achieve constant revolutions, the volume flow rates $Q \approx 40\ \mathrm{cm^3/min}$, the temperature, and two pressures p_0 and p_1, at the bypass channel entrance and exit, respectively, with a difference Δp. The channel is a slit, allowing calculation of the viscosity via Laun's single-point correction, equation (16) [15,23,24].

$$\eta(\dot{\gamma}_w) = \tau_w / \dot{\gamma}_w, \tag{16}$$

$$\tau_w = x^* \tau_a, \quad \dot{\gamma}_w = x^* \dot{\gamma}_a,$$

$$\tau_a = \Delta p h / (2l(1 + h/b)), \tag{17}$$

$$\dot{\gamma}_a = 6Q / (h^2 b),$$

$$x^* = (3/(2 + n))^{1/(n-1)},$$

where $h = 1.5$ mm, $b = 10.0$ mm, $l = 65.0$ mm are the height, breadth, and length of the bypass channel. τ_a, $\dot{\gamma}_a$ and τ_w, $\dot{\gamma}_w$ are the apparent and actual wall shear stresses and -rates. The flow behaviour indices n were taken from plate–plate viscosimetry results. All data were averaged as medians over time.

3 Results

3.1 Polymer synthesis

The syntheses resulted in materials spanning a tacticity range of $0.5 < f_{meso} \leq 1$, with an additional microbially produced commercial reference, presented as $f_{meso} > 1$ throughout the following. The synthesized PHB had molar masses of $M_n = 93 \pm 13$ kg/mol [1], and $M_w = 106 \pm 16$ kg/mol, while the isotactic microbial PHB had $M_n \approx 250$ kg/mol and $M_w \approx 660$ kg/mol, in agreement with typical values from the literature [25,26]. In this study, we re-evaluated the above-cited and previously reported [1] gel permeation chromatography data per composition f_{meso}. We found that, while the chain lengths $Z_w = M_w/(86.09\ \mathrm{g/mol})$ of our synthesized materials were on the same order of magnitude, they exhibited a continuous variation (Figure 1).

3.2 Plate–plate viscosimetry

All of the plate–plate viscosimetry data could be fitted in a satisfactory manner (Table S1) by the Herschel–Bulkley–Cross–Doolittle model, equations (8) and (9), with Carvalho et al.'s single-point correction, equation (10), provision for temperature dependence of shear thinning, equation (14), and a combined characteristic temperature T_m, equation (15).

The measured data and their fits via equation (9) showed similar progressions (Figures 2 and S1). The Kendall rank correlation coefficients τ are shown in Table S1 [27].

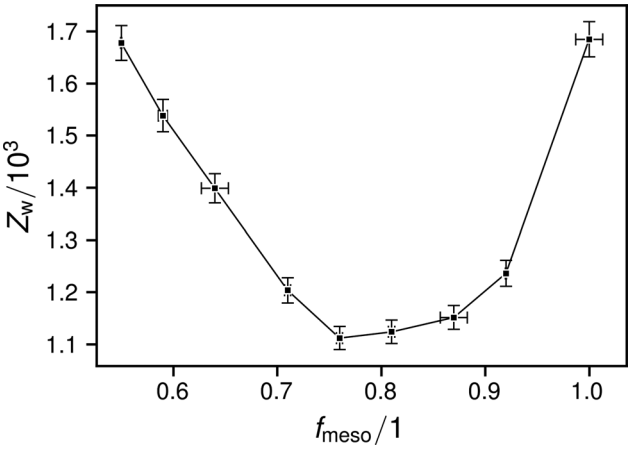

Figure 1: Weight average chain lengths of the synthesized materials.

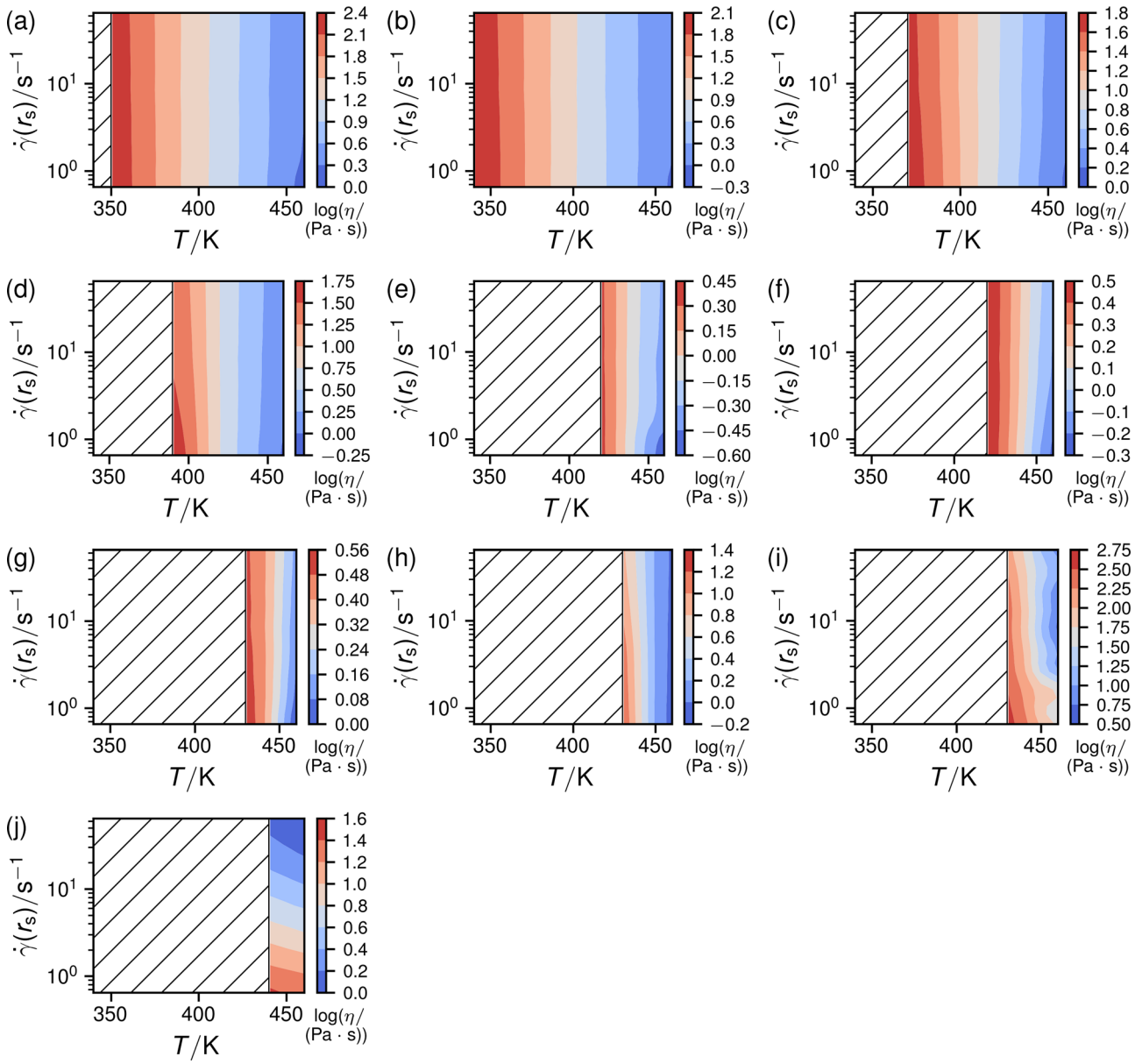

Figure 2: Logarithms of the viscosities over temperature and shear rates at the particular radii for (a) $f_{meso} = 0.55$, (b) $f_{meso} = 0.59$, (c) $f_{meso} = 0.64$, (d) $f_{meso} = 0.71$, (e) $f_{meso} = 0.76$, (f) $f_{meso} = 0.81$, (g) $f_{meso} = 0.87$, (h) $f_{meso} = 0.92$, (i) $f_{meso} = 1.00$, and (j) microbial. The presented values are medians from several measurements, see Section 2.

In Figures 3–9 and S2, the resulting fitted physical parameters are shown.

The liquid-state thermal expansion coefficients α_l follow the progression of the glassy-state α_g (Figure 3). In the microbial PHB, the ratio α_l/α_g surpasses the range 1.7 ± 0.2 determined for the synthetic compositions (Figure 4).

All synthetic PHB compositions showed Newtonian shearing behaviour $n \approx 1$ at $T \gg T_m$ (Figures 5 and 6). Shear thinning $n \ll 1$ is most significant in the long-chained isotactic microbial PHB (Figure 5). However, it also occurs in $f_{meso} = 0.71$ at low temperatures (Figure 5).

The values of A and B follow continuous trends to, respectively, lower and higher values with increasing f_{meso} (Figures 7 and 8). The values of $C \approx 1$ K for most compositions (Figure 8). Exceptions are $C(f_{meso} = 0.71) \approx 3$ K and $C(f_{meso} = 0.87) \approx 2$ K, indicating a strong temperature dependence of the flow behaviour index. Of these two, only $f_{meso} = 0.71$ exhibited a notable transitional shear stress of $\tau^* = 700 \pm 30$ Pa (Figure 9), leading to the low-temperature shear thinning shown in Figure 5. Only the long-chained microbial PHB exhibits a significant amount of yield shear stress (Figure 9). For all synthesized

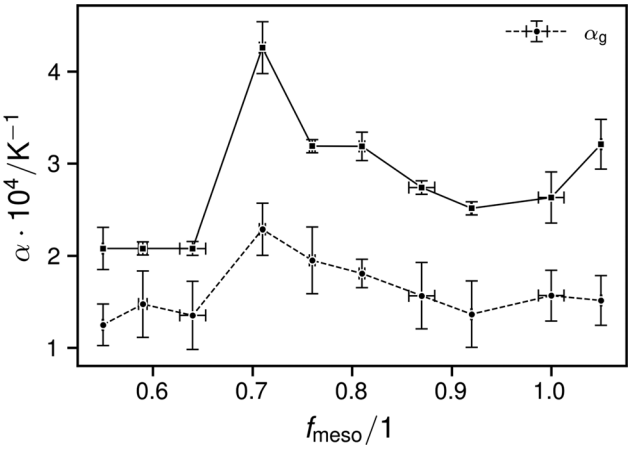

Figure 3: Thermal expansion coefficients in the liquid (squares and full lines) and glassy states (circles and dashed lines).

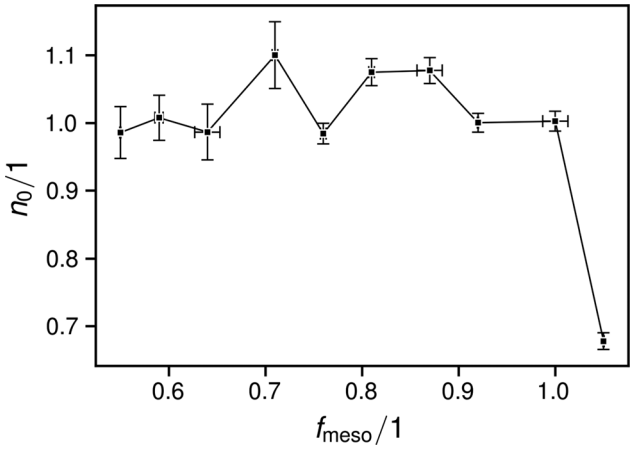

Figure 6: High-temperature limits of the flow behaviour indices.

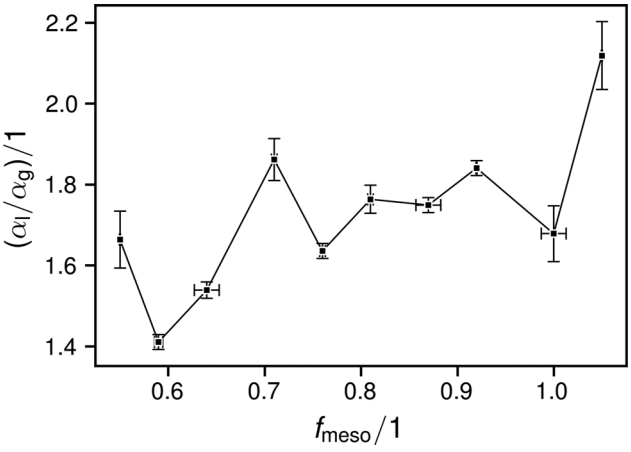

Figure 4: Ratios of the thermal expansion coefficients in the liquid and glassy states.

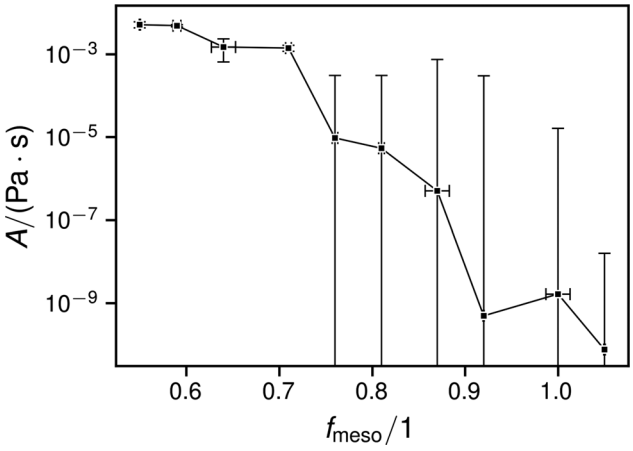

Figure 7: Doolittle scaling parameters.

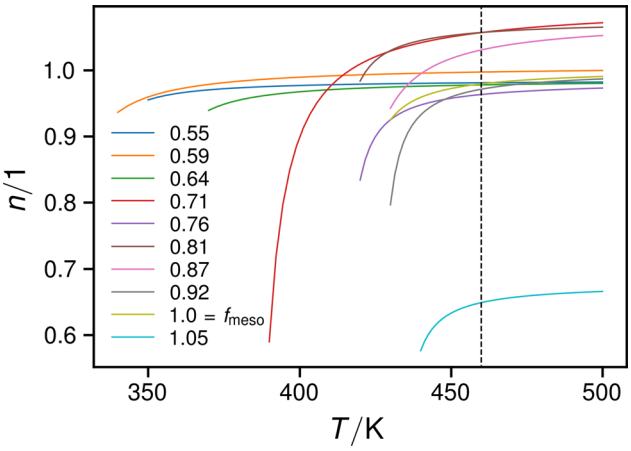

Figure 5: Progressions of the flow behaviour indices for each f_{meso} from the measured lower temperature limits, with the dashed line marking the upper limit of actual measurements.

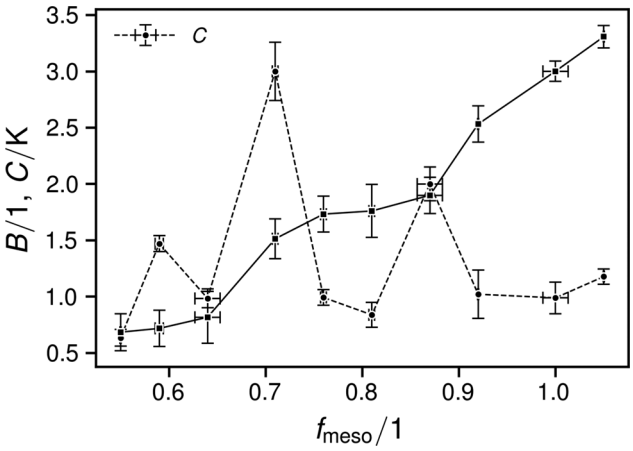

Figure 8: Doolittle exponential progression parameters B (squares and full lines) and scaling parameters to the shear thinning effect C (circles and dashed lines).

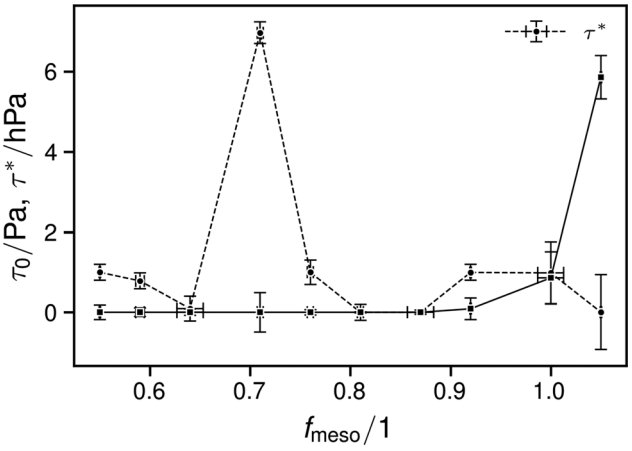

Figure 9: Yield shear stresses τ_0 (squares and full lines) and transitional shear stresses τ^* (circles and dashed lines).

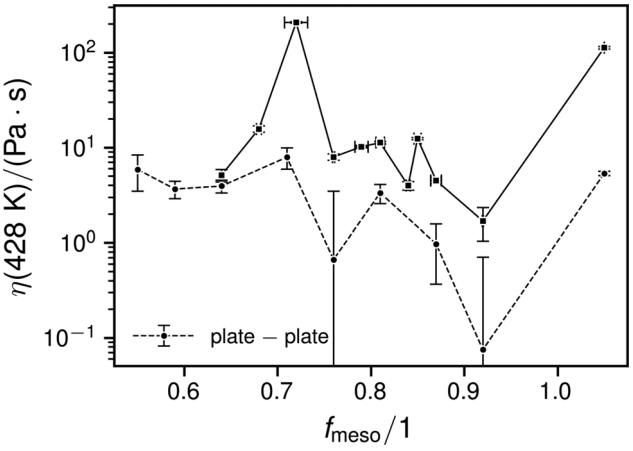

Figure 11: Viscosities calculated from slit data by equation (16) at T = 428 K and $\dot{\gamma}_w$ = 126 ± 8 s^{-1} (squares and full lines) and plate–plate data fits extrapolated to T = 428 K and $\dot{\gamma} = \infty$ (circles and dashed lines).

compositions, $\tau_0 \approx 0$, considering the attributed measures of uncertainty.

The values of T_g and T_m correspond roughly to the values determined earlier [2] (Figure S2), the latter also to the lower limits of the data presented in Figures 2 and S1. The value of $T_m(f_{meso} = 0.55)$ does not denote an actual melting point (equation (15) describes its meaning); at this composition, neither crystallization nor melting was observed [2].

3.3 Slit viscosimetry

From the extrusion machine data, we plotted the screw momenta (Figure 10) and the viscosities calculated via equation (16) (Figure 11). We were able to obtain a good qualitative correlation between the values of η from slit and plate–plate viscosimetry by extrapolating the data fits via equation (9) to an infinity shear rate.

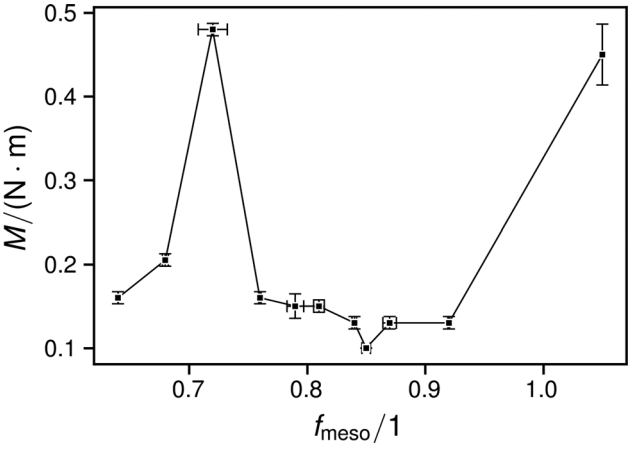

Figure 10: Medians of the momenta required for constant rotational speed of the extruder's twin-screw.

4 Discussion

4.1 Influence of the free volume

Equation (8) relates the progression $\eta_0(T)$ to the thermal expansion coefficients. As noted in the results, α_l for microbial PHB is larger proportional to the corresponding α_g than in the synthesized compositions, which we attribute to its larger molar mass (Figure 1). In support, Utracki pointed out that "in macromolecular liquids at $T > T_g$, there are several relaxation processes, often different from those of simple, low molecular weight liquids" [28]. We previously [3] considered the expansion coefficients for the crystalline/glass and rubber/liquid states of some typical polymeric glasses (Appendix I in cited book) [29]. We found that, for the considered polymers, $\alpha_l = 2.2 \pm 0.4\alpha_g$. Abdel-Hady et al. determined a rubber over glass free volume expansion ratio of 2.6 for isotactic PHB [30], while also confirming the previously determined [2] glass transition temperature of T_g = 278 ± 3. While the ratios presented in Figure 4 are lower, they follow the same qualitative trend.

The relative free volumes at the processing temperature of 428 K show a twofold progression (Figure 12): For $f_{meso} < 0.71$, V_{free} are consistently lower than 10 cl/l. For $f_{meso} > 0.71$, they decrease from a maximum value of 17 ± 1 cl/l to values ≈11 cl/l. There is no apparent correlation between V_{free} and the weight-average chain

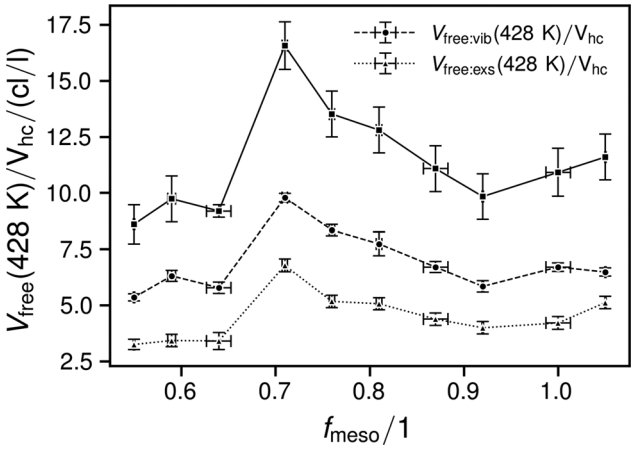

Figure 12: Relative free volumes V_{free}/V_{hc} (squares and full lines) together with their vibrational $V_{free:vib}/V_{hc}$ (circles and dashed lines) and excess contributions $V_{free:exs}/V_{hc}$ (triangles and dotted lines) at 428 K.

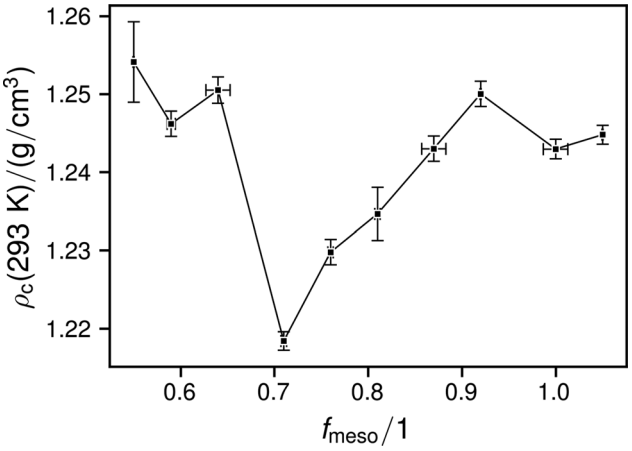

Figure 13: Crystalline phase densities at room temperature, as calculated by equation (18).

lengths Z_w. We note that the values of the relative excess free volume $V_{free:exs}/V_{hc}$ are similar, but not strictly constant, as postulated by Simha and Boyer [31]. However, considering the general variability of data by Simha and Boyer, it is unclear whether this finding constitutes an actual departure from the postulate.

We found that the values of V_{free} progress similar to the fractions of the compositions exhibiting paracrystalline disorder f_{pc} (Figure 3 in cited article [4]): With the exception of the values at $f_{meso} = 0.64$ (high f_{pc} [4], but low V_{free} determined in this work), both increase almost linearly from $f_{meso} = 1$ to $f_{meso} \approx 0.7$, then drop.

Also remarkable is the comparison between the progressions of the crystalline-phase densities ρ_c as previously determined by X-ray diffraction [4], and V_{free} determined in this work, which mirror one another horizontally. We attempted to retrace the values of ρ_c at room temperature by equation (18), with $\rho_0 = 1.3\ g/cm^3$ being the undisturbed crystal-phase density.

$$\rho_c(T) = \rho_0/(1 + \alpha_g T). \tag{18}$$

This equation utilizes the assumption that the glassy amorphous and crystalline phase expansion coefficients are similar, both being due to thermal vibrations [10]. The resulting progression of ρ_c with f_{meso} (Figure 13) follows the directly measured values (Figure 5 in cited article [4]). The ρ_c calculated via equation (18) follow a slightly steeper gradient to lower f_{meso}. In particular, the previously determined ρ_c at $f_{meso} = 0.71$ are larger, albeit with a larger uncertainty. Below $f_{meso} = 0.6$, no values were measured by X-ray diffraction for lack of crystalline phase.

The above-mentioned correlations confirm our intuitive expectation that large values of free volume in the glassy ($V_{free:vib}$) and liquid ($V_{free:exs}$) states, as well as paracrystalline disorder and reduced densities in the crystalline state in mixed-tacticity PHB have the same molecular origin, namely inter-chain mismatch due to the increasing amount of steric disturbance with increasing number of S-monomers (i.e. for smaller f_{meso}).

In general, for a single substance with fixed A and B, larger values of V_{free} correspond to lower viscosities for any given temperature, as expressed by equation (1). The progressions of the Doolittle parameters A and B show that compositions of mixed-tacticity PHB differ structurally more profoundly than expressed by the progression of their V_{free} for a given temperature. A and B reflect temperature-independent molecular interactions that scale proportionally with f_{meso}. Furthermore, the value of the glass transition temperature T_g, which contributes to V_{free} via equation (7), was practically constant for all compositions (Figure S2(a)) [2]. These points allow us to trace material properties that scale discontinuously with f_{meso} to the discontinuous progression of V_{free}. In summary, we note that the external material properties:

- twin-screw momenta required for constant-rate extrusion (Figure 10),
- viscosities determined by slit and plate–plate viscosimetry at 428 K (Figure 11),
- energies of fracture during tensile testing (Figure 4 in cited article [2])

progress similar to one another, and to the structural properties:

- values of relative free volume (Figure 12),
- paracrystalline contents (Figure 3 in cited article [4]),

- specific volumes, inverse of densities, of the crystalline phases (Figure 5 in cited article [4])

of the respective compositions. We believe that the progression of the listed material properties can be traced to structural relaxation processes enabled by large free volumes: While details vary between polymers, depending on the sizes and rigidities of the repeating units and pendant groups [32], there is a broad agreement that free volume enables chain segments to liberate, orient [32], relax [33], perform "series of jumps of flow elements to holes" [28], or conformational transitions [34], all of which can be generically referred to as relaxation processes. These arise from chain segmental mobility, and are the cause of aging in polymers below T_g [33]. They also lead to increased ductility [32], which increases impact strength, i.e. the energy of fracture [32,34], and to the general expectation that "a decrease in free volume caus[es] a decrease in impact strength" [33].

It should be added that amounts of free volume in the unstressed state do not entirely account for the material behaviour during large-strain testing: Struik found evidence to support the hypothesis "that mechanical deformations connected with segmental motion generate free volume" [33], either immediately, or by changing the equilibrium value of V_{free}.

Litt and Tobolsky proposed that in "polymers whose backbones are more rigid, due to steric hindrance or because bulky groups are part of the backbones, … molecules *may* not conform well to each other (except in an ordered crystalline phase) because the segments are bulky, skewed, or nonspherical" and "will have a large maximum unoccupied volume because of poor packing," which in turn "allows orientation of polymer segments (one or several) to relieve strain at strain levels below those at which the polymer breaks, and thus finally to give a ductile rather than brittle failure" [32]. In this work, we are considering polymer compositions that are structurally heterogeneous on the oligomeric level, due to the random sequential inclusion of R and S monomers by the catalyst during synthesis [1]. Hence, we extend the origins for large unoccupied volumes to include disorder due to mixed tacticities. Since we earlier determined that this poor packing also extends to the crystalline phase [4], we further extend Litt and Tobolsky's statements to include imperfect molecular conformations also in crystals.

We have in the past attempted to express this type of disorder as the ratio of chain segment lengths of each iso- and atactic makeup $\hat{\lambda}$ [2]. Here, we briefly return to this concept, since the progressions of $\hat{\lambda}$ for mixed-tacticity PHB (Figure 13 in cited article [2]) conform to the progressions of V_{free}, as was found to be the case for the fractional free vibrational volumes at T_g [3]. This supports the argument that measures of the lengths of chain segments of uniform tacticity (a-, iso-, syndio-) relative to one another are a viable instrument to qualitatively predict progressions of polymer properties.

Dammert et al. stated that "results from positron annihilation experiments and molecular modeling show that the tacticity of the chains in polystyrene and poly (*p*-methylstyrene) have only a very minor influence on the distribution of the free volume in these polymers" [35]. However, the materials investigated in their study were syndiotactic substances, as well as atactic ones with degrees of syndiotacticity, i.e. fractions of racemo diads f_{rac}, larger than 0.5. This is in contrast to this work, where isotactic substances were compared to atactic ones with $f_{meso} = 1 - f_{rac} > 0.5$. Intuitively, we expect the structural differences between entirely, and partially syndiotactic polymers to be smaller than between entirely, and partially isotactic ones: In the former case, the reference materials consist of chains with alternating side groups, and therefore large specific volumes that are not greatly altered by occasional meso diads. In the latter case, the reference materials comprise chains with uniform pendant group orientations, and therefore small specific volumes that we expect to be more greatly enlarged by occasional racemo diads. This is supported by the finding that "[i]sotactic poly(methyl methacrylate) has been found to be significantly less permeable to gases than the syndiotactic isomer. This can be understood in terms of the denser packing or lower free volume of the former [36]."

Simply considering the fractions of diads does not reflect their grouping into chain segment lengths, as is the case with the number $\hat{\lambda}$. However, we assume that the utility of $\hat{\lambda}$ extends only to chain segment lengths similar to the dimensions of crystallites or amorphous domains. In the following section, we consider possible effects arising from the average lengths of the polymer chains themselves, which we found to progress with f_{meso}, despite being the product of the same synthesis protocol (Figure 1) [1].

4.2 Influence of average chain lengths

Initially, Flory determined an exact relationship between viscosity and chain length in linear polyesters [37].

Differences in viscosity in non-Newtonian fluids vanish to larger shear rates, once the chains of longer polymeric species become fully aligned [38–40]. Therefore, the influence of chain length for a single type of material is reflected by the values of η_0. These can be corrected for chain length via equation (19), with proportionality constant D.

$$\eta_Z(T) = \eta_0(T)/\exp(D\sqrt{Z_w}). \quad (19)$$

We chose to compare the different compositions' viscosities at $T = 428$ K, as also used for extrusion. While we are not considering a single type of material, we observed that the values of $\log(\eta_0(428\text{ K}))$ (Figure 14), progressed similar to those of the chain lengths (Figure 1). We therefore endeavoured to minimize the influence of chain lengths via equation (19). Lacking data on η_0 for different chain lengths per composition, we minimized the normalized gradient of $\eta_Z(428\text{ K})$, based on the single values of Z_w for each synthetic composition. This was achieved with $D = 0.38$ (Figure 14).

It was not possible to achieve a uniform gradient of 0, i.e. equal values of η_Z across all compositions f_{meso}. This supports the finding that the different f_{meso} cannot be treated as a single substance. Notably, the progression of $\log(\eta_Z(f_{meso}))$ (Figure 14 being on a logarithmic scale) exhibits a twofold behaviour: A continuous increase with f_{meso} and a divergence from that behaviour at $0.64 \le f_{meso} \le 0.76$.

Considering equation (1), the continuous increase of $\log(\eta_Z(f_{meso}))$ is expected from V_{free}, which decrease with f_{meso}. With regard to the attached uncertainties, the significance of the nonlinear progression at $0.64 \le f_{meso} \le 0.76$ is questionable (Figure 14). If found to be true by future investigations, it would be a further indication for the structural dissimilarities across the investigated compositions on the oligomeric chemical level, which we earlier expressed by $\hat{\lambda}$ [2], as discussed in the previous section.

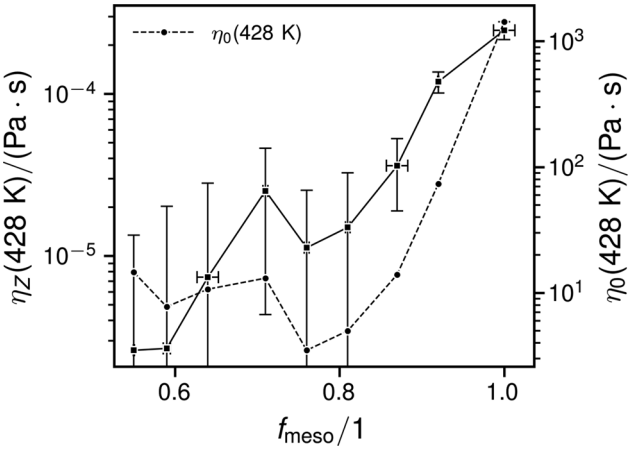

Figure 14: Chain-length corrected (η_Z, squares and full lines, by equation (19) with $D = 0.38$) and uncorrected (η_0, circles and dashed lines) zero-shear viscosities at $T = 428$ K.

4.3 Comparison with slit viscosimetry

Notably higher screw momenta were required to achieve constant flow rates Q for the compositions with $f_{meso} = 0.71$ and the microbial reference (Figure 10). These are the compositions exhibiting the maximum values of τ^* and τ_0, respectively. The M progress similar to the calculated values of η from slit viscosimetry, which in turn qualitatively match those obtained by plate–plate viscosimetry, if the values extrapolated to infinity shear rate are used (Figure 11).

We attribute the quantitative differences in η, and the corresponding $\dot{\gamma}$ ($126 \pm 8\ s^{-1}$ vs ∞) to the fact that the slit viscosimetry data were not corrected for entrance or end effects in the capillary, since it was collected during injection moulding of mechanical testing samples [2]. Such effects can be accounted for by adding a summand n_B, for Bagley, to the denominator in equation (17)[41,42]. The summand is a material property and not identical to the flow behaviour index n. It corrects for the pressure drop from the reservoir into the capillary, similar to the pressure correction via βP mentioned in Section 1. Its values are determined by measuring the pressure drops Δp as functions of the ratio of capillary length over diameter for each shear rate of interest. Then, $n_B(\dot{\gamma})$ are the absolute values of the respective intersects of linear extrapolations with the abscissa [41].

Bagley determined that for viscoelastic shear thinning materials, n_B increases with $\dot{\gamma}$ by a factor of 3 over a range of $0.5 < \log(\dot{\gamma}) < 3.5$. Furthermore, as pointed out by Mitsoulis and Hatzikiriakos, "the data points in a Bagley plot do not always fall on straight lines, and therefore extrapolation is not always possible and straightforward" [42]. They provide three main causes for curvatures in Bagley plots, all of which are related to nonlinear flow behaviour and point out that "[i]n general, at high shear stresses all the three effects are present, and the data analysis becomes even more complicated" [42]. It is therefore conclusive that, considering the attached uncertainties, the two compositions $f_{meso} = 0.71$ and microbial reference, exhibiting the strongest nonlinearity in their flow behaviour, diverge most strongly in their values η between pressureless plate–plate measurements and slit measurements.

4.4 Non-Newtonian behaviour

The values of $\eta(\dot{\gamma})$ obtained in this work for the microbial PHB at 450 K qualitatively match those reported for pure R-PHB, measured at 453 K [39]. They differ in absolute numbers, which we attribute to the single-point correction performed in this work. Choi noted that the "[s]hear viscosity decreases rapidly with shear rate because degree of chain arrangement is high in flow direction" [39]. This is a typical observation in high molecular weight linear polymers [43] and corroborated by the n for the microbial reference batch (Figure 5).

Conversely, the lower molecular masses of the synthesized PHB do not lead to pronounced shear thinning at higher temperatures. This is expected, since shorter chains in general exhibit higher chain mobility, and require less time for full alignment and disentanglement during shearing [38,40]. However, at temperatures close to T_m, the synthesized composition $f_{meso} = 0.71$ showed a pronounced shear thinning behaviour well into the measured temperature range (Figure 2(d)). This feature is accounted for by the application of equation (14) via the parameter C, and by the Herschel–Bulkley model via the parameter τ^*: In the term $(\eta_0(T)\dot{\gamma}/\tau^*)^{1-n}$ (9), the fraction of Doolittle viscosity over transitional shear stress $\eta_0(T)/\tau^*$ scales the shear rate where the viscosity departs from the Newtonian plateau.

For all synthetic compositions $f_{meso} \neq 0.71$, the lower values of τ^* mean that the gradient maximum of any transition with $n \neq 1$ is outside of the recorded $\dot{\gamma}$ (Figure 9). *Vice versa*, the value of $\tau^*(f_{meso} = 0.71)$ describes the shear thinning transition within the recorded $\dot{\gamma}$. Hence, out of the synthesized compositions, only $f_{meso} = 0.71$ exhibits both a sufficiently large τ^* and values of $n \ll 1$ at $T \approx T_m$.

A point not investigated in the scope of this work, but providing a tentative explanation is that "[f]low of molten semicrystalline polymers is also complicated by the presence of ordered structures at temperatures well above the melting point, e.g. at $T \leq T_m + 50\,^\circ$C" [28]. We earlier determined that crystallization rates drop with decreasing f_{meso} (Figure 17 in cited article), to the extent that below $f_{meso} \approx 0.8$, no crystallization processes were detected during differential scanning calorimetry runs (Figures 9 and 11 in cited article) [2]. Similarly, the melting temperatures decreased with f_{meso} (Figure 10 in cited article) [2]. As already mentioned, we also detected a continuous increase of paracrystalline disorder within the crystalline phases [4] and proposed that the elastic moduli of the amorphous- and crystalline phases become more similar with decreasing f_{meso} [2], indicating a general convergence of the behaviour of amorphous regions and regions with a degree of structural order. Combining these findings leads us to speculate that at $f_{meso} = 0.71$, within the range $T \leq T_m + 50\,^\circ$C and at low shearing rates, ordered, but non-crystalline structures may form, causing the observed shear thinning behaviour.

5 Outlook

Based on polymer melt viscosimetric data evaluated as functions of temperature and shearing rates and on previously evaluated thermal expansion data, we were able to show that direct correlations exist between the development of free volume with mixed tacticity and previously determined material characteristics, namely the energies of fracture during tensile testing, the portions of the materials exhibiting paracrystalline disorder, and the specific volumes of the crystalline phases. Thus, we traced the structural and external properties of a single type of polymer with changing tacticities, both in the solid and in the liquid state.

Foremost, it would be of interest to improve our insight into the behaviour of polymer compositions with mixed tacticities and therefore different tactic chain segment lengths through dynamic mechanical analyses, and to trace structural dynamics via simulation approaches.

Then, it will be of interest to confirm these findings in other polymer systems: One of the original aims for synthesizing mixed-tacticity PHB was to improve on the material's processing properties. Not only was this achieved by effectively lowering the melting temperature; we also found that the mechanical properties could be readily tailored. We assume that these findings can be readily transferred to other polymer systems, as well.

We further propose *in situ* investigations of structures formed in PHB melts with $f_{meso} \approx 0.7$ at temperatures just above the melting point. The nonlinear progressions of rheological parameters suggest that ordered regions might be formed, whose detection we find an intriguing prospect.

Finally, it is yet to be demonstrated that microbes can be induced to produce mixed-tacticity variants of PHB in large quantities. Due to the achievable variations in processing and resulting mechanical properties, this would represent a significant technological step towards ecologically and economically sustainable thermoplasts.

Funding information: The authors thank the Bavarian State Ministry of the Environment and Consumer Protection for

funding our work through the BayBiotech grant TLK01U-69042.

Author contributions: Daniel Van Opdenbosch: formal analysis and writing; Martin Kretschmer: investigation; Oliver Lieleg: resources and supervision; Cordt Zollfrank: funding acquisition

Conflict of interest: The authors declare no conflict of interests.

Ethical approval: The conducted research is not related to either human or animal use.

Data availability statement: The datasets generated during and/or analysed during the current study are available from the corresponding author on reasonable request.

References

[1] Haslböck M, Klotz M, Steiner L, Sperl J, Sieber V, Zollfrank C, et al. Structures of mixed-tacticity polyhydroxybutyrates. Macromolecules. 2018;51(14):5001–10.
[2] Haslböck M, Klotz M, Sperl J, Sieber V, Zollfrank C, Van Opdenbosch D. Mechanical and thermal properties of mixed-tacticity polyhydroxybutyrates and their association with iso- and atactic Chain segment length distributions. Macromolecules. 2019;42:5407–18.
[3] Van Opdenbosch D, Klotz M, Haslböck M, Zollfrank C. Free volumes and Grüneisen parameters in mixed-tacticity polyhydroxybutyrates. Macromol Chem Phys. 2021;222(15):2100087.
[4] Van Opdenbosch D, Haslböck M, Zollfrank C. Determining paracrystallinity in mixed-tacticity polyhydroxybutyrates. J Appl Crystallograph. 2021;54(1):217–27.
[5] Glasstone S, Laidler KJ, Eyring H. The theory of rate processes; the kinetics of chemical reactions, viscosity, diffusion and electrochemical phenomena. New York: McGraw-Hill Book Company; 1941.
[6] Williams ML, Landel RF, Ferry JD. The temperature dependence of relaxation mechanisms in amorphous polymers and other glass-forming liquids. J Am Chem Soc. 1955;77(14):3701–7.
[7] Doolittle AK. Studies in Newtonian flow. II. The dependence of the viscosity of liquids on free-space. J Appl Phys. 1951;22(12):1471–5.
[8] Doolittle AK, Doolittle DB. Studies in Newtonian flow. V. Further verification of the free-space viscosity equation. J Appl Phys. 1957;28(8):901–5.
[9] Wang JS, Porter RS. On the viscosity-temperature behavior of polymer melts. Rheologica Acta. 1995;34(5):496–503.
[10] White RP, Lipson JE. Polymer free volume and its connection to the glass transition. Macromolecules. 2016;49(11):3987–4007.
[11] Fox Jr TG, Flory PJ. Second-order transition temperatures and related properties of polystyrene. I. Influence of molecular weight. J Appl Phys. 1950;21(6):581–91.
[12] Fox TG, Flory PJ. The glass temperature and related properties of polystyrene. Influence of molecular weight. J Polymer Sci. 1954;14(75):315–9.
[13] White RP, Lipson JE, Higgins JS. How pure components control polymer blend miscibility. Macromolecules. 2012;45(21):8861–71.
[14] White RP, Lipson JE. Free volume in the melt and how it correlates with experimental glass transition temperatures: results for a large set of polymers. ACS Macro Lett. 2015;4(5):588–92.
[15] Kadijk S, Van Den Brule B. On the pressure dependency of the viscosity of molten polymers. Polymer Eng Sci. 1994;34(20):1535–46.
[16] Adam G, Gibbs JH. On the temperature dependence of cooperative relaxation properties in glass-forming liquids. J Chem Phys. 1965;43(1):139–46.
[17] Herschel WH, Bulkley R. Konsistenzmessungen von Gummi-Benzollösungen. Colloid Polymer Sci. 1926;39(4):291–300.
[18] Cross MM. Rheology of non-Newtonian fluids: a new flow equation for pseudoplastic systems. J Colloid Sci. 1965;20(5):417–37.
[19] Cross M. Relation between viscoelasticity and shear-thinning behaviour in liquids. Rheologica Acta. 1979;18(5):609–14.
[20] Carvalho M, Padmanabhan M, Macosko C. Single-point correction for parallel disks rheometry. J Rheol. 1994;38(6):1925–36.
[21] Newville M, Stensitzki T, Allen DB, Rawlik M, Ingargiola A, Nelson A. LMFIT: Non-linear least-square minimization and curve-fitting for Python. Astrophys Source Code Library. 2016:124.
[22] Bird RB, Armstrong RC, Hassager O. Dynamics of polymeric liquids. In: Fluid mechanics. Vol. 1. New York: Wiley; 1987.
[23] Lenk R. The Hagen-Poiseuille equation and the Rabinowitsch correction. The pressure drop in tapered channels. In: Polymer rheology. Berlin: Springer; 1978. p. 75–85.
[24] Laun H. Polymer melt rheology with a slit die. Rheologica Acta. 1983;22(2):171–85.
[25] Pachekoski WM, Dalmolin C, Agnelli JAM. The influence of the industrial processing on the degradation of poly (hidroxybutyrate)-PHB. Materials Res. 2013;16(2):237–332.
[26] Sun X, Tokuda A, Oji Y, Nakatani T, Tsuji H, Ozaki Y, et al. Effects of molar mass of poly (l-lactide acid) on the crystallization of poly [(R)-3-hydroxybutyrate] in their ultrathin blend films. Macromolecules. 2012;45(5):2485–93.
[27] Kendall MG. A new measure of rank correlation. Biometrika. 1938;30(1/2):81–93.
[28] Utracki L, Sedlacek T. Free volume dependence of polymer viscosity. Rheologica Acta. 2007;46(4):479–94.
[29] Haward RN. The physics of glassy polymers. Berlin: Springer Science & Business Media; 2012.
[30] Abdel-Hady E, Mohamed HF, Fareed SS. Temperature dependence of the free volume holes in polyhydroxybutyrate biopolymer: a positron lifetime study. Physica Status Solidi c. 2007;4(10):3907–11.
[31] Simha R, Boyer R. On a general relation involving the glass temperature and coefficients of expansion of polymers. J Chem Phys. 1962;37(5):1003–7.

[32] Litt M, Tobolsky A. Cold flow of glassy polymers. II: Ductility, impact resistance, and unoccupied volume. J Macromol Sci B Phys. 1967;1(3):433–43.
[33] Struik L. Physical aging in amorphous polymers and other materials [PhD thesis]. Technische Hogeschool Delft; 1977.
[34] Boyer R. Dependence of mechanical properties on molecular motion in polymers. Polymer Eng Sci. 1968;8(3):161–85.
[35] Dammert RM, Maunu SL, Maurer FH, Neelov IM, Niemelä S, Sundholm F, et al. Free volume and tacticity in polystyrenes. Macromolecules. 1999;32(6):1930–8.
[36] Min K, Paul D. Effect of tacticity on permeation properties of poly (methyl methacrylate). J Polymer Sci B Polymer Phys. 1988;26(5):1021–33.
[37] Flory PJ. Viscosities of linear polyesters. An exact relationship between viscosity and chain length. J Am Chem Soc. 1940;62(5):1057–70.
[38] Kröger M, Hess S. Rheological evidence for a dynamical crossover in polymer melts via nonequilibrium molecular dynamics. Phys Rev Lett. 2000;85(5):1128.
[39] Choi H, Park S, Yoon J, Lee H, Choi S. Rheological study on biodegradable poly (3-hydroxybutyrate) and its copolymer. J Macromol Sci A. 1995;32(sup1):843–52.
[40] Xu X, Chen J, An L. Shear thinning behavior of linear polymer melts under shear flow via nonequilibrium molecular dynamics. J Chem Phys. 2014;140(17):174902.
[41] Bagley E. End corrections in the capillary flow of polyethylene. J Appl Phys. 1957;28(5):624–7.
[42] Mitsoulis E, Hatzikiriakos SG. Bagley correction: the effect of contraction angle and its prediction. Rheologica Acta. 2003;42(4):309–20.
[43] Kobayashi K, Nagasawa T. Crystallization of sheared polymer melts. J Macromol Sci B Phys. 1970;4(2):331–45.